Meteoritics & Planetary Science 39, Nr 2, 247–265 (2004)
Abstract available online at http://meteoritics.org

Early fracturing and impact residue emplacement: Can modelling help to predict their location in major craters?

Anton KEARSLEY,[1*] Giles GRAHAM,[2] Tony McDONNELL,[3] Phil BLAND,[4] Rob HOUGH,[5] and Paul HELPS[6]

[1]Department of Mineralogy, The Natural History Museum, Cromwell Road, London SW7 5BD, UK
[2]Institute of Geophysics and Planetary Physics, Lawrence Livermore National Laboratory, California, USA
[3]Planetary and Space Sciences Research Institute, The Open University, Milton Keynes, MK7 6AA, UK
[4]Department of Earth Science and Engineering, Imperial College London, London SW7 2AZ, UK
[5]Museum of Western Australia, Francis Street, Perth, Western Australia 6000, Australia
[6]School of Earth Sciences and Geography, Kingston University, Kingston-upon-Thames, Surrey, KT1 2EE, UK
[*]Corresponding author. E-mail: antk@nhm.ac.uk

(Received 30 June 2003; revision accepted 15 December 2003)

Abstract–Understanding the nature and composition of larger extraterrestrial bodies that may collide with the Earth is important. One source of information lies in the record of ancient impact craters, some of which have yielded chemical information as to the impacting body. Many deeply eroded craters have no remaining melt sheet or ejecta yet may contain impactor residue within basement fractures. The emplacement mechanism for fractionated siderophile residues is likely to be gaseous, although, melt droplets and some solid materials may survive. For breccia- and melt-filled fractures to contain extraterrestrial material, they must form very early in the impact process. Most current numerical models do not dwell on the formation and location of early major fractures, although, fractures in and around small craters on brittle glass exposed to hypervelocity impact in low Earth orbit have been successfully simulated. Modelling of fracture development associated with larger craters may help locate impact residues and test the models themselves.

INTRODUCTION

Recent estimates suggest that extraterrestrial bodies capable of creating km-scale craters impact Earth's surface with a frequency of perhaps one in 100,000 years, although, the flux of similar-sized but more fragile asteroids, which suffer atmospheric disruption, may be substantially higher (Bland and Artemieva 2003; Grieve and Dence 1979). The number of terrestrial craters available for study is severely restricted by their erosion and burial by geological processes (Hughes 2000), complicating interpretation of the nature, origin, and flux of extraterrestrial bodies that have impacted. The witnessed and well-documented historical record of impacts is limited to the scale of relatively small craters such as the Sikhote Alin crater field (Krinov 1966). Beyond the observation that ordinary chondrite meteorites dominate find and fall collections and may, therefore, represent the bulk of the recent (<1 Ma) Earth-crossing asteroid population, we have little realistic assessment of the origin of major impacting bodies in the geological past, where they may come from within our solar system, and whether their fluxes have changed through time. Recognition of the composition of ancient impacting bodies from their remnants in craters and ejecta provides the only "ground-truth" data for understanding what has happened outside of our very limited span of direct observation. To date, there is published evidence of diverse types of impactors (e.g., Horn and El Goresy 1980; Palme 1982; Kyte and Brownlee 1985; Mittlefehldt et al. 1992; Kyte 1998; McDonald et al. 2001; McDonald 2002).

There are practical problems in attempting to link composition of extraterrestrial bodies to crater formation. In the case of a major impact, where there has been little reduction in bolide velocity due to atmospheric transit, the conversion of kinetic energy into shock and decompressional heating may be sufficient to dismember, melt, and vaporize the majority of the impacting body and, therefore, leave no pristine remnant as evidence of origin. Instead, material may be mixed with large volumes of target rock and may be widely dispersed as a minor component within impact spherules or within and adjacent to the crater as discrete particles or sheets of melt glass. Such characteristic products of impact are

relatively vulnerable to dissolution and diagenetic transformation, resulting in their loss as prominent signs of catastrophe.

Inevitably, and especially where good access to surface outcrop permits, an immediate prospect for location of impactor residue will be the vicinity of the crater. Many of the better-exposed craters are found in arid areas, subject to extremes of cold or heat, and remote from populous habitation. In a field investigation in and around a crater, duration may be limited by logistic support: time and other available resources become major constraints. It becomes important to know where the most effective places may be to look for materials that could tell the type of object responsible for the crater. Modelling of crater-forming processes has been remarkably successful in illuminating events on time scales and physical scales that cannot be directly observed and visually described. Can numerical modelling also help to predict the locations in which recognizable bolide residue could be found?

LOCATIONS OF RESIDUE PRESERVATION

The nature of an extraterrestrial body that has created a terrestrial impact crater through a hypervelocity impact can sometimes be determined by the collection of disrupted and shocked impactor as loose fragments or within small bodies of impact melt from the ground surface in and around the crater, e.g., iron meteorites from the vicinity of the Barringer crater, USA (Rinehart 1957); Henbury, Australia (Spencer and Hey 1933); Sikhote Alin, Siberia (Krinov 1966); meteoritic debris and impact glasses from Lonar, India (Frederiksson et al. 1979); Wabar, Saudi Arabia (Spencer and Hey 1933); and Monturaqui, Chile (Sanchez and Cassidy 1966). Meteoritic debris may be found in sedimentary sequences deposited around oceanic impact events, e.g., from the Eltanin impact (SE Pacific), sampled from the deep sea (Kyte and Brownlee 1985; Kyte 2002). In these cases, attribution of an impacting body to a particular origin is relatively straightforward as petrographic sectioning and geochemical analysis are likely to reveal diagnostic features, although with modification by shock. If a major melt component is still preserved at the crater, for example, as glass bombs within the suevites at Ries in Germany (Morgan et al. 1979; Pernicka et al. 1987); as a substantial discrete melt body as at Popigai in Siberia (Masaitis 1994); or in core as at Chicxulub in Mexico (Koeberl et al. 1994), then materials suitable for bulk trace element or isotopic analysis may also be relatively easy to collect. These sometimes permit recognition of an extraterrestrial signature (Grieve 1992), even if subtle, as there can be widespread dissemination of impactor residue through the melt or even possible preservation of parts of the bolide in the form of inclusions, as seen at Morokweng in the Republic of South Africa (Koeberl et al. 1997; Koeberl and Reimold 2003). Unfortunately, if an impact feature has been substantially modified by subsequent erosion, e.g., Sierra Madera in Texas (Howard et al. 1972), it may prove more difficult or impossible to find chemical residue from the bolide. Characteristic large-scale impact-related structures (e.g., central uplifts and ring-synclinoria) may remain, with diagnostic shock indicators such as shatter cones, planar deformation features, and high pressure mineral polymorphs (French 1998), yet the ejecta blanket and any impact melt body are lost.

FRACTURES AND RESIDUES

It is intriguing to note that some eroded structures have been shown to retain extraterrestrial residues and debris derived from higher structural levels emplaced within fractures, e.g., the quartzite-clast-bearing "granophyre dykes" intruded as sharply defined sheets into granulite facies basement rocks in the center of the Proterozoic impact structure at Vredefort in the Republic of South Africa (Koeberl et al. 1996) and residue-bearing breccias in rim rocks at Roter Kamm in Namibia (Degenhardt et al. 1994) and possibly at Woodleigh in Australia (Koeberl et al. 2001). For residue to be able to penetrate along these fissures, brittle regime fracturing must occur either very early in the crater-forming process, at a stage when abundant bolide material is still available and has not been ejected, or during extensional fracturing at the apex of an uplifted central zone, beneath a melt-sheet or residue-rich fall-back deposit from which mixed bolide and target melt can be intruded.

Very early fracture development and polymict breccia emplacement in displaced crater floor rocks has been reported recently from Chicxulub by Wittmann et al. (2003). In some craters, there is also evidence of substantial outward motion of target debris along major radial fracture systems. The "offset dykes" of the southern margin at Sudbury contain substantial quantities of breccia believed to have been generated along major fault zones during crater wall collapse (Scott and Spray 2000) and intruded by melt tapped from the main crater pool, although these structures have also acted as conduits for later migration of more fractionated melts (Wood and Spray 1998). However, the brief description by Spray (2001) of the outward transport of extremely large basement clasts along some "dykes" to positions km away from their parent location does imply that these major fractures must be created earlier than the melt intrusion along fault zones "inflating" during the substantial displacement of crater wall collapse. Remnant outward-directed, compressive, "reverse" motion can also been seen in the displacement of well-defined reflectors across the outermost faults visible in seismic reflection profiles of the Chicxulub crater (Morgan and Warner 1999) and within the finely resolved deep structure of the Silverpit crater (Stewart and Allen 2002). Reactivation of major faults and consequent "normal" displacement during modification of the crater profile due to gravitational collapse

may reduce, eliminate, or even transfer downthrow and, thereby, modify the apparent offset due to earlier phases of motion. Major subhorizontal movements have been implicated in the radial outward (and inward) transport of material responsible for the growth of peak rings (Morgan et al. 2000). Both field observations (e.g., seismic profiles with stratigraphic control from gold exploration drilling in the ring synclinorium at Vredefort by Brink et al. 1997) and recent numerical models (Kenkmann et al. 2000) suggest that these movements are relatively late-stage modifications to crater structure. However, it is very difficult to account for the reverse sense of motion seen in the more distal high-angle faults at Chicxulub without implying an early origin for these planes of movement. In fact, detailed structural analysis of major displacement zones in well-exposed crater basement is a relatively recent field of study (e.g., Kenkmann and von Dalwigk 2000). Nevertheless, Shoemaker and Kieffer (1974) hinted that breccia-filled dykes occur at the Barringer crater; Stöffler et al. (1988) recognized the significance of basement fracturing and breccia dyke emplacement in the early development stages of large craters; and Kremenetsky and Yushko (1997) give a brief account of major breccia-filled fractures at depth in a Russian astrobleme. In recent numerical models (e.g., O'Keefe et al. 2001; Collins et al. 2002), such structures are beginning to assume great importance as simulated features, despite substantial difficulty in their modelling, especially in the light of the computational requirements necessary to achieve adequate spatial resolution.

There appear to be a number of outstanding questions. How often and exactly where are major fractures created during the very early (compression to excavation) phases of crater growth? In what state is residue emplaced, by what mechanism, and how widespread is residue within fractures? What is the best way to recognize emplaced residues? Can numerical models that predict early brittle fracturing give guidance as to where we should look? Do residues from later-stage central uplift fractures, rich in melted target rocks, differ from those emplaced in early fractures?

SAMPLES AND ANALYTICAL INSTRUMENTATION

Geochemical analysis of bulk rock impactite samples can yield subtle evidence of extraterrestrial input. Extensive studies by Koeberl and other authors (excellent summaries are given by Koeberl [1998, 2001]) have demonstrated that isotopes of the first row transition elements, and also particularly of the platinum-group elements (PGE), can show the presence of even very small quantities of meteoritic material (e.g., Koeberl et al. 1994, 2002). In many of the examples studied to date, there may be no obvious visible sign of impact-derived carrier minerals in hand specimen or petrographic thin section, although textural features may show that high pressure shock processing has occurred. Polished sections of some materials, produced for electron microprobe analytical studies, can reveal μm-scale diagnostic textures and compositions. Distinctive, fine-scale (μm) native siderophile element metal segregations occur within melt-rich impactites at the surface of a number of smaller (km-scale) craters and have been reported within melt-poor breccias sampled at depth from the Ries crater (El Goresy and Chao 1976; Chao and El Goresy 1977).

To compare the characteristics of siderophile segregations of undisputed impact origin, we have examined polished sections of vesicular impactite glass samples collected as loose particles on the ground surface from 4 craters: Lonar in India; Wabar in the Empty Quarter of Saudi Arabia; Monturaqui in Chile; and Barringer in Arizona, USA. We have also analyzed polished sections of the Canyon Diablo coarse octahedrite iron meteorite (from the meteorite strewn field associated with the Barringer crater) and polished sections of breccia from 1059.1 to 1059.25 m-depth in the 1973 Nordlingen borehole core material, from Ries in Germany. As the geochemical fractionation of siderophile elements may be partly controlled by oxygen fugacity (for example, changing the oxidation state of iron and its subsequent behavior with respect to migration into silicate melts), we have also examined impactite metals from the oxygen-poor lunar environment, represented by a polished section of the Dar al Gani 400 lunar anorthositic breccia meteorite (NHM P10727) and a carbon-coated chip of the Dar al Gani 262 lunar anorthositic breccia meteorite.

The large (1.4 cm) impactite bead from the Barringer crater was purchased in 1985 from a collection made by H. Nininger. It is very similar to the specimens lodged at the Natural History Museum, London (NHM) (BM1967,55), but no detailed locality information is available. It is a pale brown vesicular glass (Fig. 1a), rich in zoned olivine and pyroxene crystals, with calcite vesicle fills and containing occasional clasts of sandstone that are unmelted but highly shocked with quartz grains displaying well-developed planar deformation features. In the vesicular glass, and among abundant "Ballen" silica patches, complex subspherical metal and metal sulfide droplets occur, usually of 30–40 μm diameter (Fig. 1b). The metals have diverse compositions (Table 1) with enrichment of both nickel and cobalt (Fig. 2) relative to the primary mineralogy of the impacting body, the Canyon Diablo octahedrite (Table 2).

The Wabar impactite specimen (BM 32, 1161) was collected from the crater field in 1932 by H. St. J. Philby and is part of a substantial collection lodged at the NHM. It is a polymict vesicular glass with areas of transparent frothy silica glass mixed with dark blue-black iron-rich silicate glass (Fig. 3a) containing convoluted trains of tiny (sub-μm) spherical droplets of nickel-rich metal and inclusions of partially melted lithified argillaceous sandstone (Fig. 3b).

The specimen from Monturaqui is part of a collection purchased in 2001 from R. Hartman and is now lodged at the

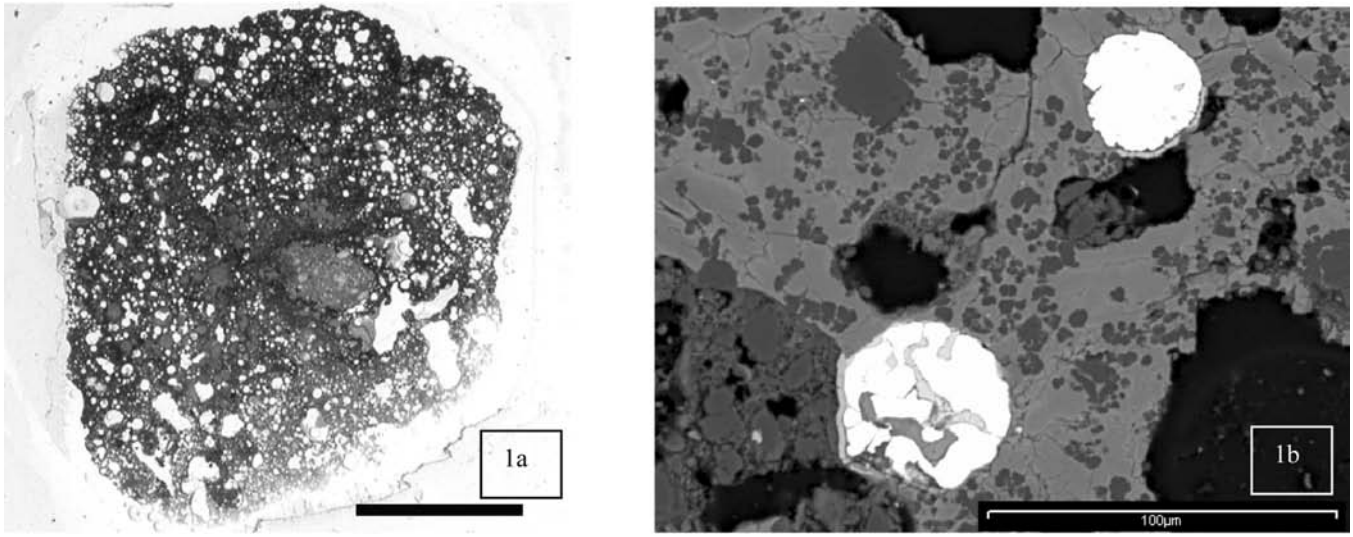

Fig. 1. a) Transmitted light photograph of a polished section of vesicular glass in a cm-scale melt droplet. Vesicles appear pale, and a clast of shocked but unmelted calcite-cemented sandstone is visible near the center. The scale bar is 5 mm; b) backscattered electron image (BEI) of a typical area of the Barringer melt droplet. The white is nickel- and cobalt-rich metal, the pale grey is glass and calcic clinopyroxene, and the dark grey is silica. The scale bar is 100 µm.

Table 1. Analyses of Canyon Diablo meteorite components by WDS.[a]

Wt%	Kamacite mean	n = 15 SD	Taenite mean	n = 7 SD	Schreibersite mean	n = 10 SD
Fe	93.31	0.82	66.84	4.39	50.89	14.80
Co	0.86	0.44	0.34	0.08	0.33	0.14
Ni	6.57	0.73	31.2	3.72	34.27	10.26
Si	0.07 bdl	0.14	0.08 bdl	0.04	bdl	0.06
P	0.11 bdl	0.15	0.05 bdl	0.04	13.88	4.67
S	0.03 bdl	0.10	0.05 bdl	0.13	bdl	0.05
O	0.32	0.13	0.75	0.15	0.89	0.31
Total	101.06	1.39	99.13	2.28	100.06	0.46

[a]The strewn field of this group IA coarse octahedrite iron meteorite surrounds The Barringer crater, and it is likely to be representative of the impacting body. Note relatively low cobalt throughout, homogeneity of kamacite and schreibersite compositions, and variable nickel content of taenite.

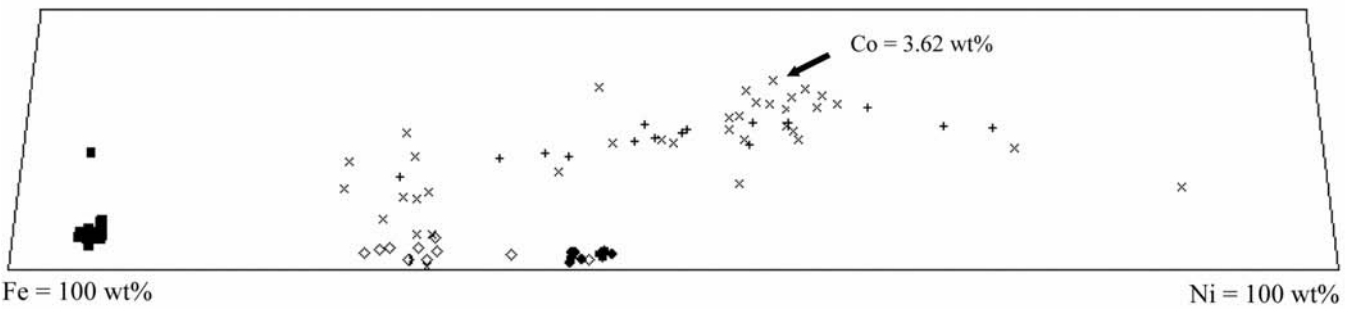

Fig. 2. Triangular plot of normalized weight percentage of iron, nickel, and cobalt in components of the Canyon Diablo meteorite and metal particles within the Barringer crater melt droplet (1a). The vertical scale is stretched to show variation in cobalt. The highest cobalt content plotted is 3.62 wt%. Key: ■ = kamacite in Canyon Diablo (20 analyses by WDS); ◆ = schreibersite in Canyon Diablo (9 WDS); ◇ = taenite in Canyon Diablo (13 WDS); × = metal particles in Barringer melt droplet (37 EDS); + = metal particles in Barringer melt droplet (15 WDS).

Table 2. Analyses of the Barringer crater impactite metals by EDS.[a]

Wt%	BS2.3	BS2.5	BS3.4	BS4.2	BS5.2	BS6.2	BS7.5	BS8.1	BS9.2	BS10.4
Fe	43.7	37.4	37.2	38.0	41.7	63.0	48.3	55.2	56.0	22.4
Co	2.9	3.1	3.32	2.9	2.6	2.5	3.0	2.9	2.0	2.8
Ni	53.9	60.0	59.7	59.9	56.9	36.3	49.3	41.4	41.8	74.6
Si	bdl	bdl	bdl	bdl	bdl	bdl	bdl	bdl	bdl	bdl
P	bdl	bdl	bdl	bdl	bdl	bdl	bdl	bdl	bdl	bdl
S	bdl	bdl	bdl	bdl	bdl	bdl	bdl	bdl	bdl	bdl
O	0.6	bdl	1.2	0.7	0.6	bdl	bdl	bdl	0.8	0.8
Total	101.1	100.5	100.4	101.5	101.8	101.8	100.6	99.5	100.6	100.6

[a]Note the wide range of Fe:Ni ratios with nickel reaching higher concentrations than in any meteoritic component in Canyon Diablo.

NHM. Although it is known that all the Monturaqui samples were collected from the immediate vicinity of the crater, no further location details are available. The sample is a brown vesicular glass rich in granitic rock clasts and meteoritic metal (Fig. 4a), similar to material described by Bunch and Cassidy (1972).

The sample from Lonar was collected as a loose particle from immediately outside the crater rim in 1999 by Eric Dransart, who kindly donated a sample, now lodged at the NHM (BM 2002, M.60). It is a black, cinder-like polymict vesicular glass (Fig. 5a) primarily composed of quench-crystallized dendritic pyroxenes set in a feldspathic glass matrix with vesicular feldspar glass bodies and subspherical vesicular silica droplets, both of mm-size (Fig. 5b). The predominant glass composition, and the presence of clasts containing highly fractured pyroxene that are both veined and enclosed by maskelynite of labradorite composition, demonstrate an origin from the groundmass of basalts that dominate the crater locality. The vesicular feldspar glass is probably derived from coarser basaltic phenocryst material, and the less-common vesicular silica glasses from the thin sedimentary sequences interbedded within the lava pile.

Backscattered electron imagery (BEI) and qualitative and quantitative X-ray microanalysis of native metals were carried out on a JEOL JSM840 scanning electron microscope (SEM) fitted with an Oxford Instruments exL Pentafet energy dispersive X-ray spectrometer (EDS), a JEOL 5900LV SEM with an Oxford Instruments INCA Pentafet EDS, and a Cameca SX50 Wavelength Dispersive electron microprobe (WDS). The size of the individual metal particles studied was wide-ranging, from mm- to μm-scale. Most are not homogeneous and contain internal compositional domains of less than 10 μm in diameter. Many are irregular masses of 2–5 μm, a scale smaller than the effective interaction volume of an electron beam operated at more than 10 keV with a beam current in excess of 10 nA, which is necessary for wavelength dispersive X-ray analysis (WDS) of minor and trace element chemistry. Analysis of many particles was, therefore, not possible by WDS, and quantitative microanalysis by EDS was employed but limited to major element composition with detection limits no better than 0.2% by weight for the first row transition elements. Comparison of WDS and EDS analyses of the same area of larger grains showed that the two techniques gave analyses with excellent correspondence. An accelerating voltage of 20 kV was used throughout with a beam current of 2 nA on the JEOL 840, 1.57 nA on the JEOL 5900, and 20 nA on the Cameca SX50 for major elements. Microanalysis standards were a suite of high purity metals, synthetic pure end member fayalite, natural pyrite, synthetic scandium phosphate, and natural apatite (the main standards suites from Oxford Brookes University and the Natural History Museum). For the larger metal grains silicon, phosphorus, and sulfur, the first row transition metals gallium, germanium, iridium, and gold were analyzed by WDS using TAP, PET, and LiF crystals. Gold and iridium were below detection limit at 120 sec count time and 200 nA current, and our analyses for Cr, Cu, Ga, and Ge are to be published separately as part of a larger study of siderophile trace element fractionation in impactite native metals. We intend to prepare ultra thin sections by precise focused-ion beam milling for further in situ analysis of extremely small grains using proton induced X-ray emission (PIXE) and secondary ion mass spectrometry (SIMS).

OBSERVATIONS OF METALLIC RESIDUES IN MELTS AND IN FRACTURES

Our impactite samples show that that μm-scale metallic residue is inimately associated with other impact products found within silicate and carbonate melt glass (Figs. 1b, 3c, and 4d), within vesicles (Fig. 5c), between brecciated rock fragments (Fig. 4b), or as thin coatings on target rock clasts (Figs. 3b, 3c, and 3d). Electron microprobe analyses of residual metal may sometimes show a typical meteoritic kamacite metal Fe:Ni ratio of ~10:1 (Table 3, Wabar impactite S4.2, mean of 3 analyses; Table 4, Monturaqui impactite, analysis S4). Metal grains within silicate-dominated impact melt are usually too small (sub-mm) to show the coarser metallographic textures that may have been present in the impacting body, and the metal may appear homogeneous in backscattered electron images, although, a few (Fig. 4c) do show poorly preserved fine-scale crystalline texture. Microprobe analyses often show that substantial modification of metal composition has occurred during and after the impact, for example, in the small metal droplets in the Barringer crater melt when compared to the primary bolide

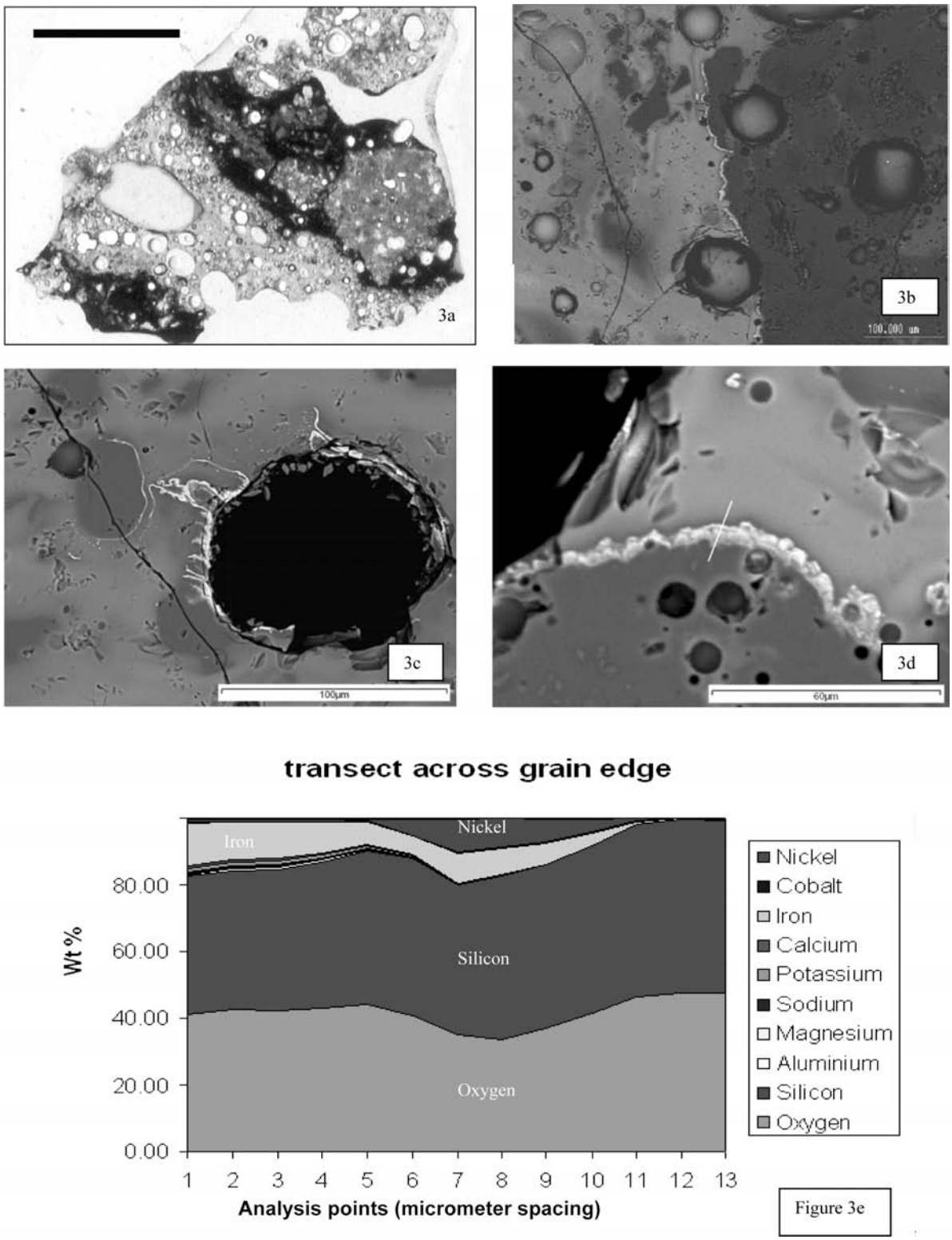

Fig. 3. a) Transmitted light photograph of polished section. Note the variation in color and degree of vesiculation. The scale bar is 1 cm; b) BEI of contact between iron-rich vesicular melt (pale grey at left) and partially-melted sandstone clast (dark grey at right). There is a bright band of nickel- and cobalt-enriched metal at contact. The scale bar is 100 µm; c) BEI of nickel-rich metal as sub-µm droplets in trains surrounding silica grain and vesicle. The scale bar is 100 µm; d) BEI with line of analysis points across metal-rich band. The scale bar is 60 µm; e) plot of compositions (EDS) at points along line shown in Fig. 3d. Note the nickel concentration at the boundary between iron-rich glass (left) and silica grain (right).

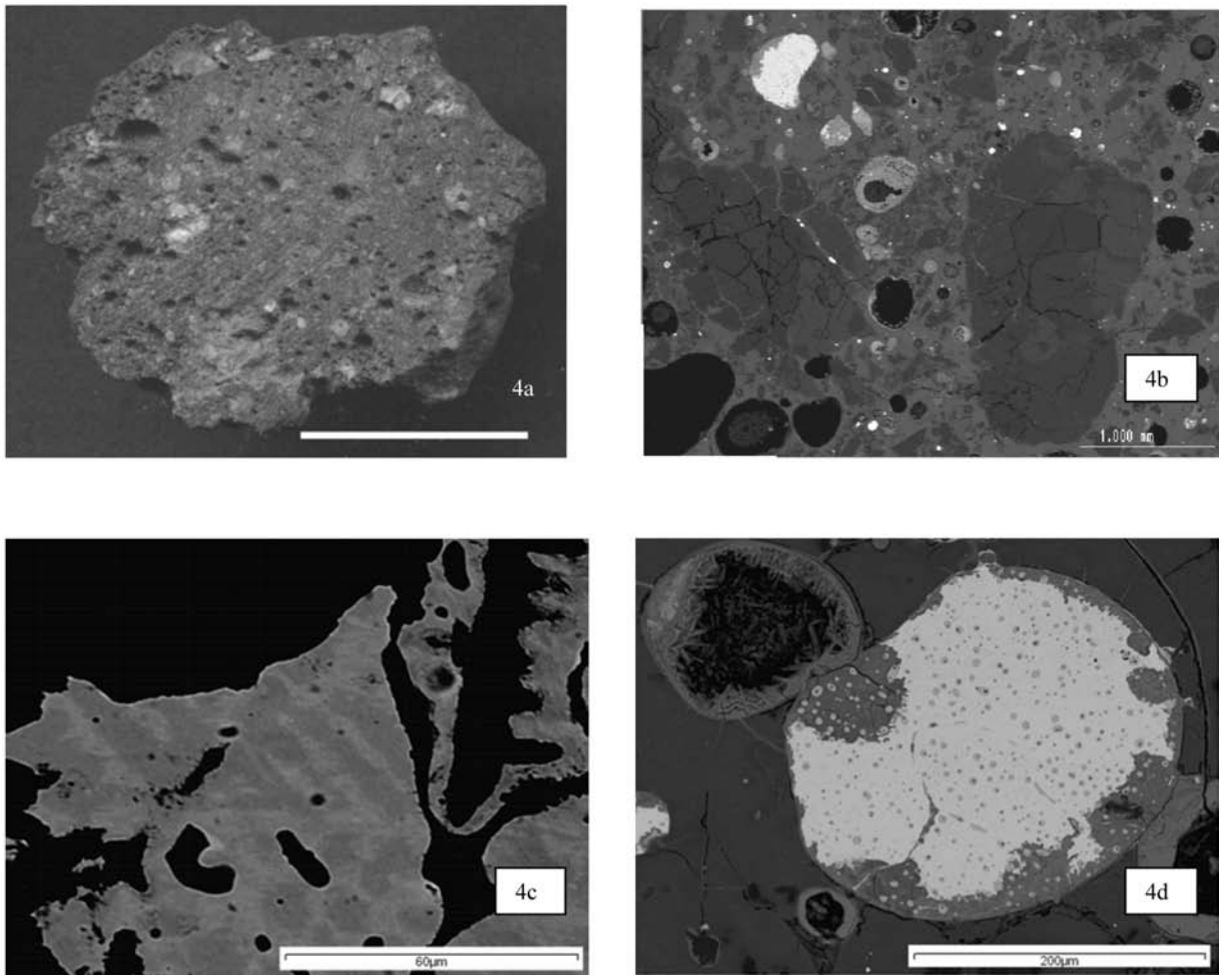

Fig. 4. a) Sawn section of grain. The scale bar is 1 cm; b) BEI of polished section showing granite clasts (quartz and albitic feldspar appear dark grey, potassium-rich alkali feldspar mid grey) veined by silicate glass (pale grey) and metallic residue (white). The scale bar is 1 mm; c) BEI of metal grain with crystallographic control of composition. The pale areas are relatively nickel-rich. The scale bar is 60 µm; d) BEI. The metal pale, the iron sulfide is mid-grey, the dark grey areas at the edge are iron oxide weathering. The scale bar is 200 µm.

composition of the Canyon Diablo group IA iron meteorite (Fig. 2). In a single small impactite specimen, there may be metallic grains of widely differing texture and composition with localized enrichment of nickel and cobalt (Tables 2, 3, and 4), presumably a consequence of oxidized iron loss into silicate-rich melt (Fig. 3e).

The variable extent to which the first row transition elements fractionate may be demonstrated in a comparison of metal-bearing impact melts from the Barringer, Wabar, Monturaqui, and Lonar craters. In backscattered electron images of polished sections through melt droplets of cm-size from Barringer, we have found segregation of nickel- and cobalt-rich metal (Table 2) into tiny droplets (typically 20 µm, the bright areas in Fig. 1a) within a groundmass of vesicular glass from which iron-rich silicates have grown. Similar metals have been reported by Brett (1967), Kelly et al. (1974), and Mittelfehldt et al. (1992). Quantitative EDS and WDS analyses of our larger melt droplets reveal that there is little or no pristine meteoritic metal. The distribution and composition of the PGE in the near-crater impactites at Barringer may prove to be no less interesting, especially as there is growing evidence of their fractionation during impact processing, which may hold clues as to the physical conditions of fireball and plume (Schmidt et al. 1995).

At Wabar, the vesicular silica-rich glass contains abundant tiny droplets of nickel-rich meteoritic metal and iron sulfide (Hörz et al. 1991). These produce a characteristic blue color, similar to that described in Zhamanshin by Zolensky and Koeberl (1991). Along the contacts between glass and partially melted, weakly lithified sandstone clasts (Figs. 3b and 3d), and also marginal to vesicles (Fig. 3c), we have observed accumulation of nickel- and cobalt-enriched metal (Fig. 3e). This suggests that similar behavior to that at Barringer has begun, with loss of iron through oxidation and incorporation into silicate melt, accompanied by the creation of tiny (sub-µm-scale) nickel-rich metal droplets and localized concentration of nickel and cobalt at the interface with pre-existing silicate solids but with termination at an

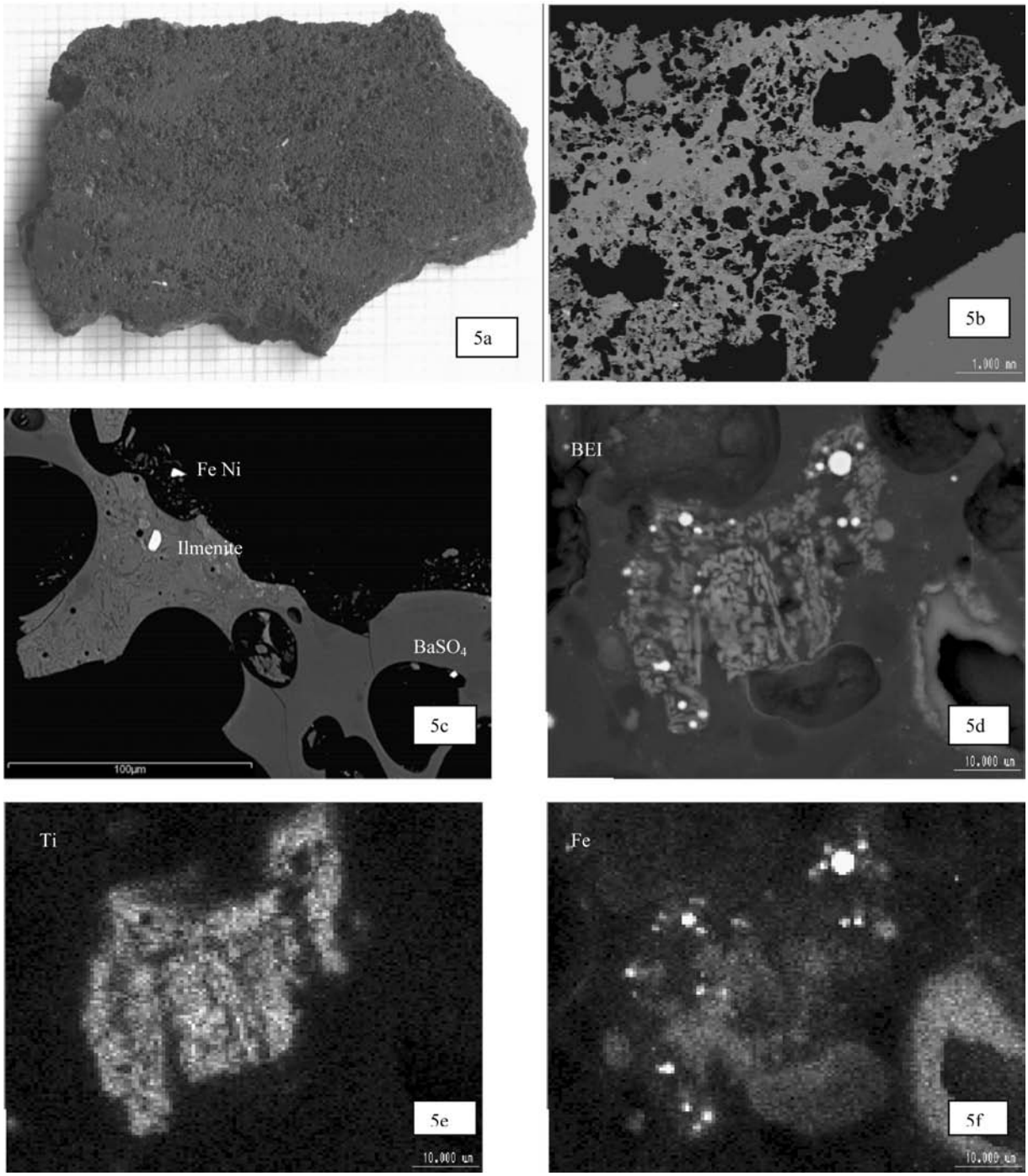

Fig. 5. a) Sawn slab. Background scale of 1 mm squares; b) BEI of polished section. The darker grey vesicular patches at top right are silica glass. At the top left is vesicular plagioclase feldspar glass. The scale bar is 1 mm; c) BEI reveals bright grains of barium sulfate (diagenetic), ilmenite (basaltic), and iron-nickel metallic residue. The scale bar is 100 µm; d) BEI of bright metallic iron droplets located within denatured iron-titanium oxide grain; e) EDS X-ray map of Titanium distribution in and around denatured Fe-Ti oxide; f) EDS X-ray map of iron distribution. Note the spherical droplet. The scale bar in (d), (e), and (f) is 10 µm.

earlier stage, before aggregation into the larger (20 µm) immiscible droplets characteristic of Barringer (Fig. 1b).

Intimate relationships between metallic residue and target lithologies are also seen in backscattered electron images and X-ray maps of polished sections from Monturaqui, in which shocked granite clasts within melt are veined with injected iron-rich silicate melt that often contains droplets of iron-nickel metal and iron sulfide (Fig. 4b). Microprobe analyses reveal that there is little metal fractionation apparent within most of the larger (mm-scale)

Table 3. Barringer crater and Wabar metal droplets.[a]

	Barringer					Wabar				
Wt%	S1 (5)	S2 (5)	S4 (8)	S6 (5)	S7 (10)	S4.2 (3)	S5.1	S5.4	S5.3	S7.2
Fe	22.7	38.8	10.8	52.7	68.4	88.0	73.7	57.8	54.2	88.1
Co	2.3	2.5	1.5	2.4	1.3	0.8	1.0	5.4	4.1	1.2
Ni	72.2	57.0	85.3	43.4	28.2	9.6	21.5	38.8	36.6	10.2
P	bdl	bdl	bdl	bdl	bdl	bdl	0.3	0.3	bdl	bdl
S	0.6	0.7	bdl	0.9	bdl	bdl	bdl	bdl	bdl	bdl
Mg	bdl	bdl	bdl	bdl	bdl	bdl	0.5	bdl	0.2	0.6
Al	bdl	bdl	bdl	bdl	bdl	bdl	0.5	bdl	bdl	bdl
Si	0.3	0.2	0.5	bdl	0.6	0.3	1.4	bdl	1.9	0.3
Ca	0.2	bdl	0.3	bdl	bdl	bdl	bdl	bdl	0.2	bdl
O	1.6	0.7	1.2	0.6	1.1	1.5	1.2	0.3	2.6	bdl
Total	99.9	99.9	99.6	100.0	99.6	100.2	100.1	102.6	99.8	100.4

[a]Quantitative EDS analyses of impactite metal grains.

Table 4. Monturaqui crater and Lonar crater metal droplets.[a]

	Monturaqui					Lonar				
Wt%	S4	S7	S20.1	S20.2	S20.3	S25.4	S11.1	S17.1	S21.3	S31.1
Fe	88.8	61.7	54.2	59.1	69.1	96.9	51.2	87.8	56.9	1.4
Co	1.0	2.1	2.1	2.3	2.6	bdl	bdl	1.1	0.4	bdl
Ni	8.8	35.2	42.5	37.3	28.3	bdl	44.5	6.1	40.7	92.5
P	0.4	bdl	bdl	bdl	bdl	bdl	bdl	bdl	bdl	bdl
S	bdl	bdl	bdl	bdl	bdl	bdl	bdl	bdl	bdl	bdl
Mg	bdl	bdl	bdl	bdl	bdl	bdl	bdl	bdl	bdl	0.2
Al	bdl	bdl	bdl	bdl	bdl	bdl	bdl	bdl	bdl	1.0
Si	0.1	0.3	bdl	0.2	bdl	0.5	0.3	0.4	0.3	1.8
Ca	bdl	bdl	bdl	bdl	bdl	bdl	bdl	0.2	0.2	0.4
O	0.7	0.7	0.7	0.7	0.7	2.2	1.1	1.4	0.9	2.0
Total	99.8	100.1	99.6	99.5	100.8	99.6	97.1	97.0	99.4	99.3

[a]Quantitative EDS analyses of impactite metal grains.

metallic bodies in the glass at Monturaqui (Fig. 4c and Table 4, analysis S4) despite textural evidence of melting in some (Fig. 4d). The tiny droplets of μm-scale, emplaced within fractured clasts and dispersed in the glass, are markedly more nickel-rich (Table 4).

BEI of impact glasses from Lonar show that they are rather different in the distribution of metal residue, suggesting that target lithology may play an important role in controlling the style and location of impact residue retention. Lonar was excavated in a sequence of basaltic lava flows and interbedded sedimentary units (Frederiksson et al. 1973). The vesicular melt glass reflects a mixture of components processed and mixed at high temperature resulting in a polymict agglomeration of glasses (Fig. 5b). Inclusions with shocked mineral textures, such as veining of fractured pyroxene by plagioclase feldspar glass, demonstrate an impact origin for the vesicular material. We have found metal as small (<10 μm) irregular grains within vesicles (Fig. 5c) and with a wide range of iron to nickel ratios (Table 4).

The co-existence of different nickel-rich, μm-scale native metals (Fig. 6) is a feature that appears unique in nature to impactites and must reflect extremely fine-scale heterogeneity of physical conditions within the impact environment and the rapidity of solidification without opportunity for equilibration. Fractionation and deposition of metals following intense and rapid heating can be observed in the laboratory adjacent to pits created by laser ablation for trace element and isotopic analysis. However, it is certainly not safe to assume that all siderophile segregation and precipitation is directly related to very high temperature "impact" processes. Target rocks may be sites of mineralization, either by pre-existing normal terrestrial fluid circulation within basement or by hydrothermal convective circulation driven through fractured basement by residual heat from a large impact (e.g., Osinski et al. 2001). The frequent association of lake development by flooding of crater depressions, e.g., at Tswaing crater in the Republic of South Africa in the modern day or at the Ries crater during the Miocene, may yield a ready supply of almost closed-system fluid within which anion activity can build to levels adequate for metal ion complexing and redistribution. Especially where target rocks are reactive (e.g., carbonate-rich), this can lead to deposition and fractionation of different metals, although, usually as sulfide, carbonate, and oxide phases rather than native metals.

The low local oxygen fugacity within the impact-heated

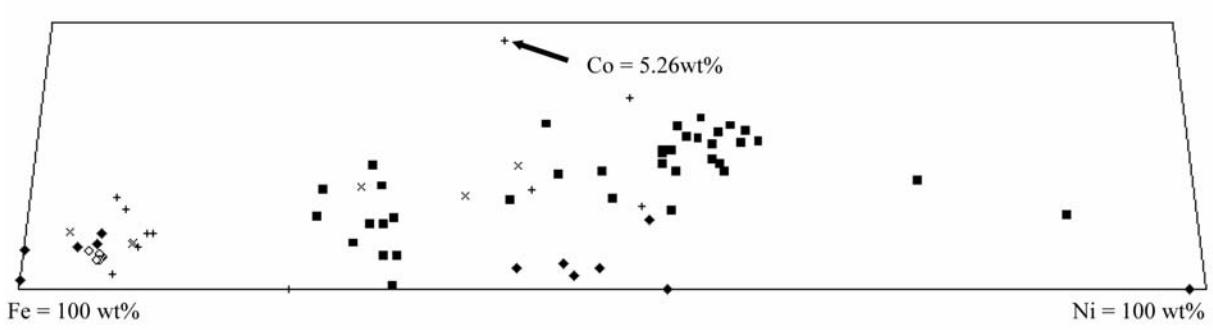

Fig. 6. Triangular plot of normalized percentage of iron, nickel, and cobalt in impactite metals and meteoritic kamacite. All data are from quantitative EDS. The vertical scale is stretched to show variation in cobalt. The highest cobalt content plotted is 5.26 wt%. Key: ■ = Barringer metal particles; ◆ = Lonar metal particles; ◇ = Canyon Diablo kamacite; × = Monturaqui metal particles; ＋ = Wabar metal particles.

area is shown by another paragenesis of native metal. If iron-bearing oxides are present in the target rocks, such as the titanium-iron oxide accessory minerals in the basalts of the Lonar crater, iron-rich metal may also be generated by dissociation of minerals such as ilmenite (Figs. 5d, 5e, and 5f). The low nickel content, characteristic titanium content, and the close proximity of melt droplets to remnant titanium oxides can be used to distinguish this metal from true impactor residue.

At the Ries crater, variably brecciated and foliated basement rocks (granitoid igneous rocks and amphibolite metamorphic rocks) are exposed in scattered outcrops and quarries (Hüttner and Schmidt-Kaler 1999). Less-deformed microgranites may contain thin breccia or pseudotachylite veins and occasional broader (few cm) breccia dykes that contain clasts derived from higher stratigraphic levels in the target sequence (e.g., at Langenmuhle). More extensive exposure of veined basement rocks occurs in the quarry at Unterwilfingen, but here, as in most other localities, subaerial weathering following submergence within a saline and carbonate-rich lake for several Ma has resulted in dissolution, transport, and replacement of minerals, especially in the finer breccia matrix. Coarser basement breccias, such as those exposed near Nördlingen at Meyer's Keller, have been extensively degraded. Siderophile-rich segregations reported from within these types of lithology (El Goresy and Chao 1976) may be difficult to interpret due to the complex post-impact history, especially if it cannot be proven that hydrothermal or sub-lacustrine diagenetic alteration has not occurred. We have examined fresh basement rocks, cored from approximately 1 km-depth in the Nördlingen 1973 borehole. Cut surfaces of the core reveal extensive fragmentation and mixture of lithologies at all scales between cm and μm. The rock is dominated by quartz and alkali feldspars, with relict textural features of granitic igneous rock (Fig. 7b), although the presence of occasional deformed evaporate clasts of calcium sulfate with minor barium sulfate (Fig. 7a) testifies to inclusion of some of the overlying sedimentary sequence and a lack of pervasive aqueous alteration either at the time of metal deposition or afterward. Trains of dismembered monazite grains (Fig. 7c) demonstrate that much of the brecciation in the sample is associated with local shearing. The interstitial voids between angular quartz and feldspar grains contain dispersed tiny nickel grains (Fig. 7d) the abundance of which can reach levels equivalent to 660 ppm nickel in the whole rock, as determined from automated point-counting of high resolution X-ray maps. Iron is distributed as a thin oxide coating that is pervasive on silicate grain surfaces within fractures, although this may be a secondary alteration product.

What, therefore, is the likely mechanism of transport responsible for emplacement of distinctive impactite metals? Is there an interaction of target rock with metal melt or with metal vapor? The well-defined separation into two components, a vesicular ferrous-iron dominated mafic silicate-with-glass assemblage (well-preserved in young impactites but vulnerable to diagenetic reworking) and immiscible tiny, nickel-dominated metal droplets, suggests that the process, although vigorous and efficient, must have been extremely rapid, obviously occurring before solidification of the glass. The localization of nickel deposition as a very fine film around melting clasts and around vesicles within the glass at Wabar implies that metal was dispersed either as vapor or melt droplets on a sub-μm-scale before contact with the target-rock silicates. Some studies (Yakovlev and Basilevsky 1994) have suggested that siderophile elements can be vaporized by the intense heating associated with impact, although the efficiency of this mechanism has been questioned by Schnabel et al. (1999), whose simulation of the impact at Barringer suggests much melting but little vaporization of the Canyon Diablo bolide. Unfortunately, preliminary data reported by Sugita et al. (2003) show that laboratory experiments may not provide good analogues for heating during impact, as laser heating exceeds the temperatures attained during real impacts and generates substantially more vapor. Surprisingly diverse elemental assemblages can be linked to impact heating even where relatively high oxygen fugacity cannot exert control on

metal availability for inclusion in silicate melts (Housley 1979). To determine whether fractionation effects are mainly due to reaction in an oxygenated atmosphere or to selective vaporization, we have examined the lunar anorthosite breccia meteorites Dar al Gani (DaG) 262 (Bischoff et al. 1998) and Dar al Gani 400 (Zipfel et al. 1998). In DaG 400, substantial particles of metal are common, with grain sizes of tens of μm and a major element composition (Fe 89.2; Co 1.3; Ni 9.5 wt%) indistinguishable from meteoritic kamacite. The particles are comparable in size to the fine breccia clasts and are likely to be remnants of an impacting body, although the inter-fingering of their margins with silicates grown from the interstitial melt (Fig. 8) suggests high temperature processing, perhaps as melt. In DaG 262, we have observed μm-scale sub-spherical droplets of metal (Fig. 9b), with composition comparable to meteoritic kamacite but found as immiscible droplets in glassy melt veins and lining vesicles (Fig. 9a), clearly demonstrating that they have been emplaced into vein-filled fractures from a fluid, probably vapor, phase. The survival of a meteoritic Fe:Ni ratio in these tiny droplets is in stark contrast to the modification of composition seen in small metal droplets within terrestrial impactites (for example, in the droplets of Fig. 3c) and implies that reaction with the surrounding silicate melt host has not occurred. This is likely to be a consequence of the lack of an oxidizing environment in the vacuum of the lunar surface, which prevents generation of ferrous (and ferric) iron. Our observation of the terrestrial occurrence of unusual metal within vesicles at Lonar, in injected veins at Monturaqui, and within breccias at Ries may also imply injection of mixed vapor, melt, and fragments into target-rock fractures, with siderophile segregation occurring both in a vapor phase and during oxidation and reaction with the host rock. We suggest that the occurrence of the distinctive nickel-rich grains at Ries implies that modified impactor components were emplaced into deep target rock, uplifted as a central ring during crater modification. This occurrence may be compared with the emplacement of more substantial amounts of extraneous breccia, subjected to higher temperature bulk-rock modification and target rock melting, seen in the shocked-quartzite bearing "granophyre dykes" at Vredefort (Koeberl et al. 1996). Whether native metal segregation occurs only from primary metal in the impactor or may be a more general feature of impact processing of other meteoritic solids, as implied by the generation of metal droplets from silicate precursors in laser ablation experiments, is unknown. Other residue materials that could be emplaced within fractures, such as silicate glass films, are very likely to be unstable and subsequently may be dissolved or recrystallized, leading to apparent loss from the site of emplacement. It is not surprising that fine metallic residue can be recognized as dispersed among surficial impact-generated deposits when the bolide was dominated by an iron-nickel alloy such as seen at the Barringer crater, yet, the location of nickeliferous metal processed from a meteoritic source within fractured clasts and bedrock demonstrates that residue can be emplaced to depth on both fine (mm) and coarse (100 m to km) scales. Native metal residues are relatively easy to locate by their high electron backscatter coefficient when compared to surrounding silicate minerals, but it is likely that other, less prominent residue compositions may be emplaced into fractures by a similar mechanism and may be more typical of metal-poor projectiles.

OBSERVATION AND MODELLING OF FRACTURE DEVELOPMENT IN VERY SMALL CRATERS

As part of a separate suite of studies (e.g., Graham et al. 2000), we have made an extensive survey of μm- to mm-scale impact craters on brittle, laminated glass solar cells exposed to hypervelocity collision of micrometeoroids (typical velocity 25 km s^{-1}) during exposure at 600 km altitude in low Earth orbit (LEO) on the Hubble Space Telescope (HST). The majority of sub-mm impact features contain a hemispherical "melt-pit," a proxy for the transient crater (Fig. 10a), within the surface of which is usually found impactor residue (Fig. 10b). The residue may be mafic silicate and miscible with the melted solar cell glass; it may be droplets of immiscible iron sulfide or, occasionally, meteoritic metal with no evidence of fractionation of iron from nickel during the impact of kamacite in the vacuum of space, although this process has been reported by Miura et al. (1999). The crater melt pit is almost always surrounded by pervasive shattering, a zone of surface spallation, and a relatively wide zone of more broadly spaced fractures that extend to more than 5 times the transient crater radius (Fig. 10c). These fractures have previously been considered relatively late-stage features (McDonnell et al. 2001), later than generation of the narrower spall zone (which is due to extensional failure close to the glass surface), and were believed to slowly propagate well after the passage of the shock wave through the laminate structure. However, our repeated observation of probable micrometeoroid fragments within these solar cell glass fractures (Fig. 10d) suggested that the fractures must be formed early, while projectile material is still in motion. Although some residue may have been emplaced in a gaseous or molten state, our laboratory experiments have revealed that even delicate, volatile-rich residues can be emplaced into fractures around small craters on brittle substrates (Figs. 11a and 11b). May the complex shape and internal heterogeneity of micrometeoroid structure and composition cause partitioning of strain and enhance survival of some melted particulate debris?

We have also simulated small impacts using "buckshot" mineral grains within a discarding sabot, accelerated to approximately 5 km s^{-1}, in a light-gas gun. A wide range of brittle target materials have been used including laminated solar cell glass, silicon, germanium, rock, and mineral surfaces (Fig. 11). Unless detachment of the central crater pit has occurred due to well-developed cleavage in the

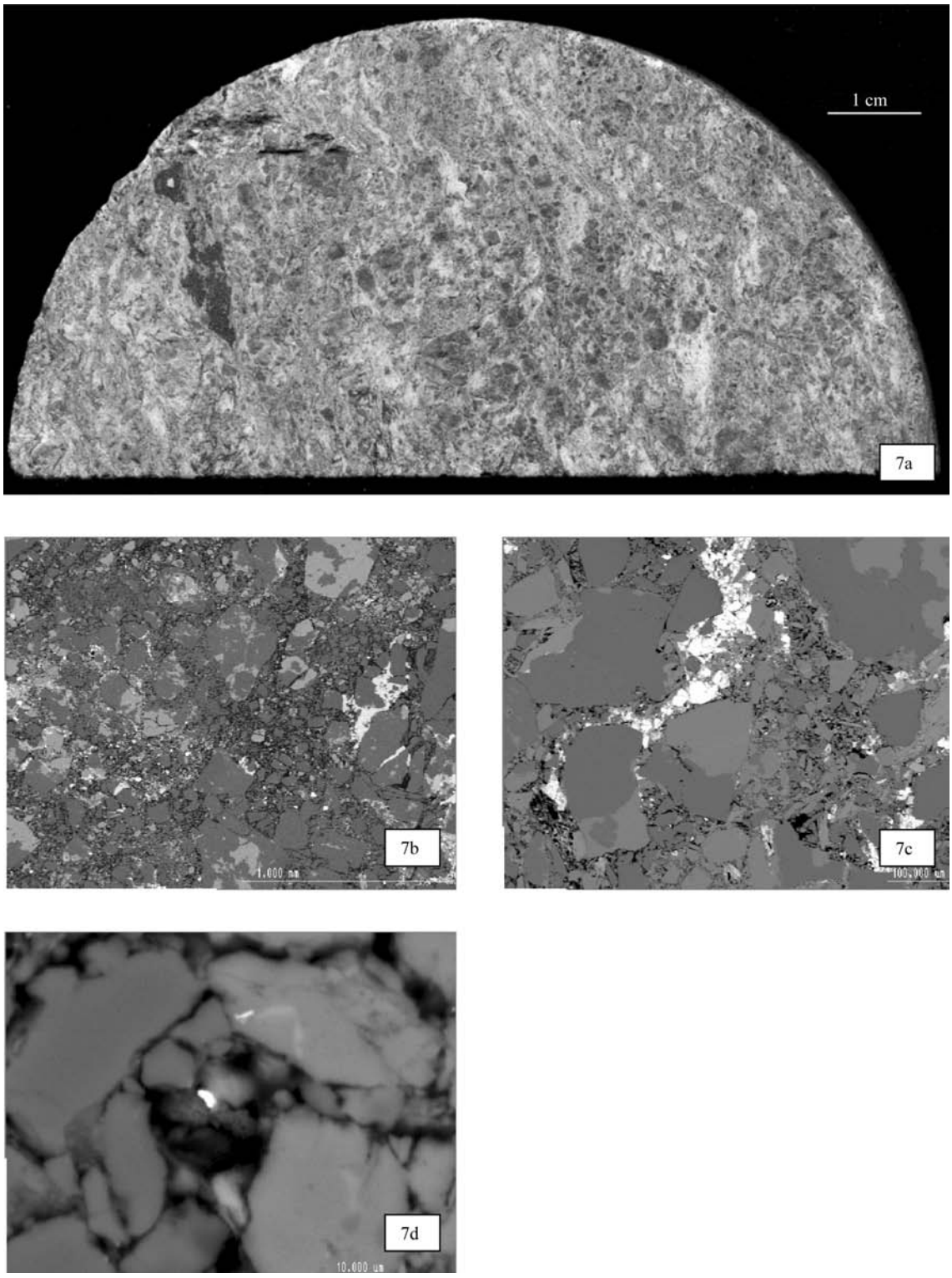

Fig. 7. Cross section of core from 1973 Nordlingen borehole, depth 1059.1 m, Ries crater: a) the very dark areas are calcium sulfate, the mid-grey areas are alkali feldspar, and the pale areas are quartz and brecciated granite; a pervasive fabric cuts through the rock, which is almost pseudotachylite in places. The scale bar is 1 cm; b) BEI of polished section. The pale grey areas are heavy minerals including zircon and monazite, the mid-grey areas are potassium-rich alkali feldspar, and the dark grey areas are quartz and albitic feldspar. The scale bar is 1 mm; c) BEI of a dismembered monazite grain. It is very pale within the image, is a light-rare-earth phosphate accessory mineral, is common in granites, and due to relative softness, has been "ball-milled" between durable quartz and feldspar grains. The scale bar is 100 μm; d) BEI of metallic nickel grain (bright) in small void within granite breccia, Nordlingen 1973 borehole, 1059 m.

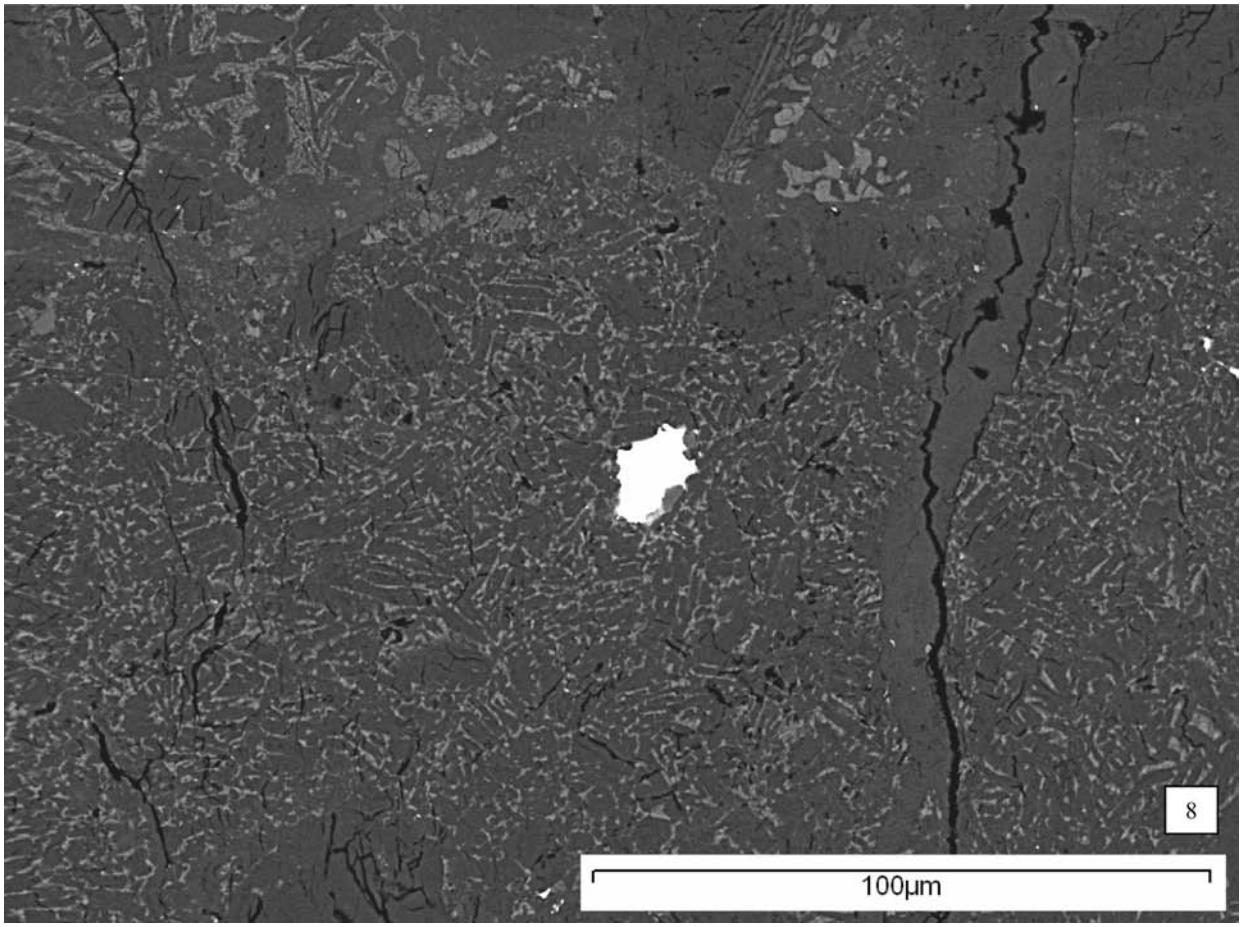

Fig. 8. BEI of metallic particle. Note the complex shape of the edge in contact with surrounding silicates. The scale bar is 100 μm.

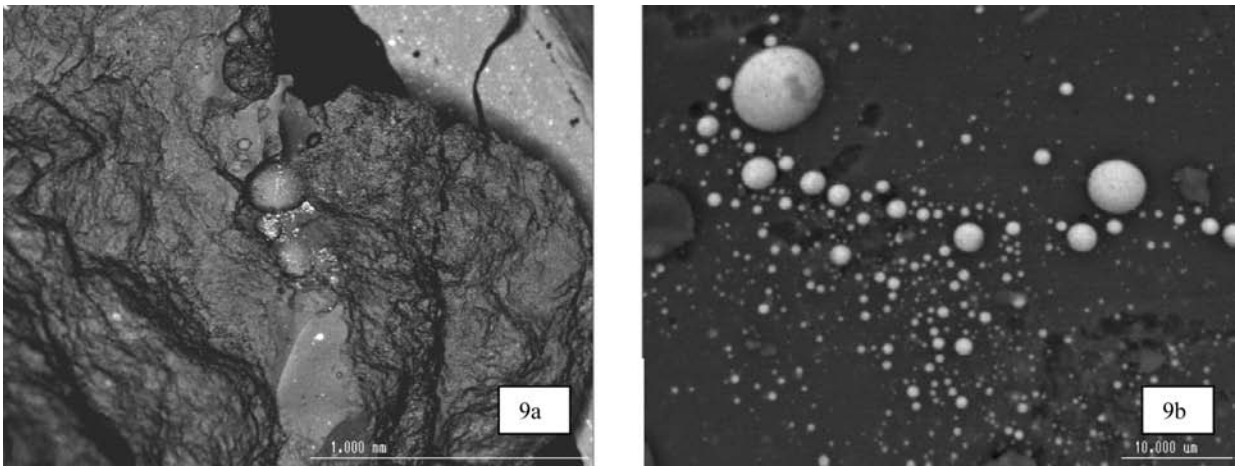

Fig. 9. a) BEI of broken surface shows glassy and vesicular silicate melt vein cutting breccia. The bright spots are metal. The scale bar is 1 mm; b) BEI of interior of vesicle in melt vein shows metal droplets of diverse size but apparently identical composition. The scale bar is 10 μm.

underlying substrate, as may occur on silicon (Taylor et al. 2001), the majority of the impact residue is found as melted or condensed droplets within a thin melt sheet solidified on the surface of what is effectively a preserved transient crater profile, closely comparable to features seen in LEO impacts. Laboratory craters may also contain particulate impactor residue in conchoidal fractures (extending to the target surface) and in radial fractures. In some small craters on rock, there is evidence of outward radial transport of target material (Fig. 11b).

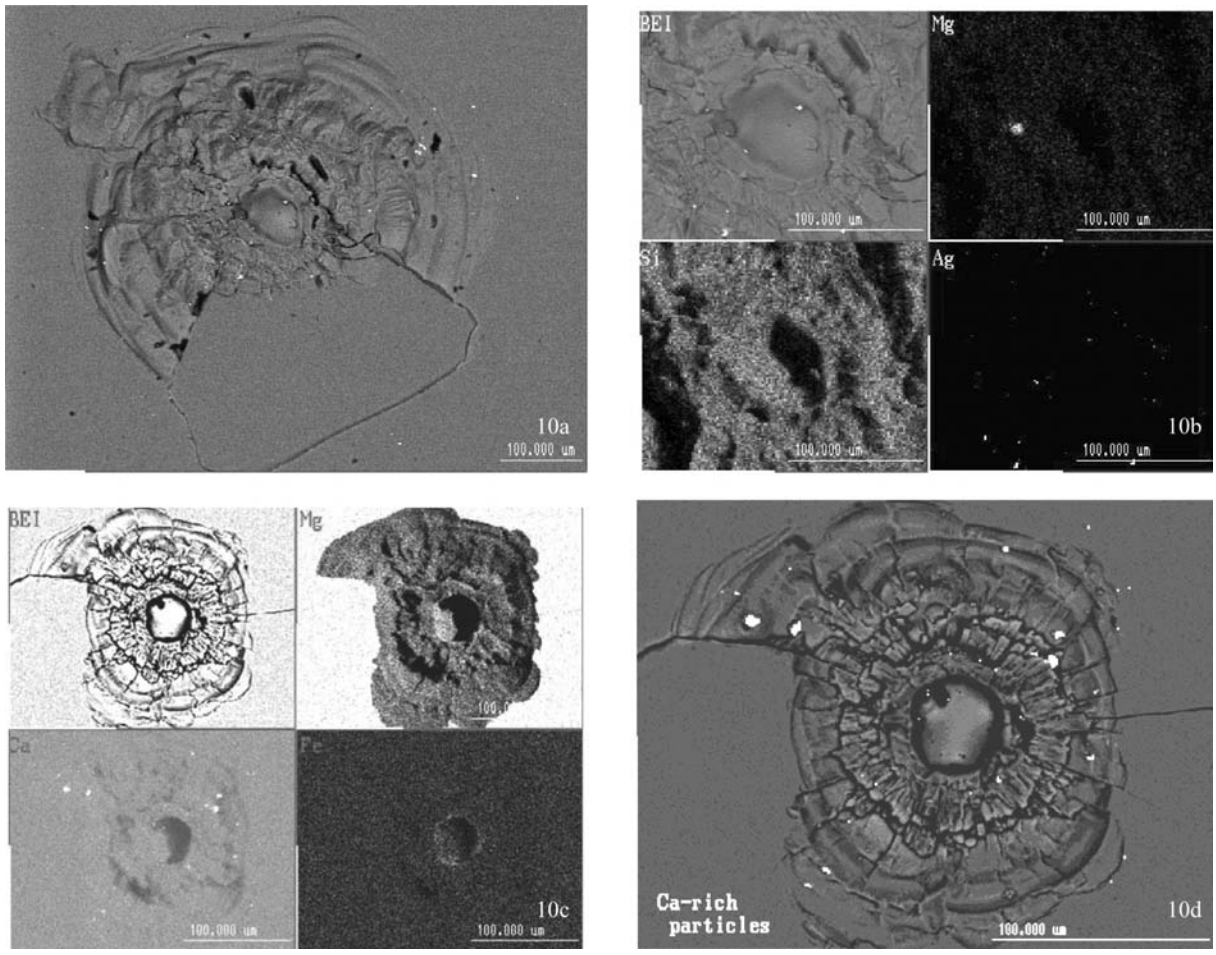

Fig. 10. a) BEI of impact crater on borosilicate glass surface of a solar cell. Note the smooth hemispherical "melt pit" marking the position of the impact, broad conchoidal zones of fracturing and spallation, and two scales of radial fractures. The scale bar is 100 μm; b) EDS X-ray maps show a solitary olivine grain with target-derived silver debris. The scale bar is 100 μm; c) BEI and Xray maps of micrometeoroid LEO impact crater on HST solar cell glass. The residue within the central melt pit is a magnesium-rich silicate. The scale bar is 100 μm; d) combined BEI and EDS X-ray maps show calcium-rich particles (probably carbonate) in radial shatter zone and conchoidal fracture zone, implying early formation of fractures. The scale bar is 100 μm.

NUMERICAL MODELING OF SMALL CRATER FRACTURES

The impetus to perform modelling of solar cell craters came from the necessity to explain what seemed to be an anomalous relationship between residue and target in these craters in that the existing physical models predicted loss of all the projectile material by ejection of vapor and melt before the formation of the cracks in which we had actually observed the projectile remnants. Numerical models of small hypervelocity impacts on brittle glass materials have been described in detail by Taylor et al. (1999). A similar approach has been employed recently for small impacts upon ceramic and concrete substrates by Clegg et al. (2002) using the Johnson-Holmquist failure model and the Rankine plasticity model (as described in Clegg and Hayhurst [2000]) of the AUTODYN-2D non-linear dynamic analysis software marketed by Century Dynamics. AUTODYN-2D can apply Eulerian and Lagrangian processors to model deformation at a wide range of strain rates and in a wide range of substrates, such as the use of the smooth particle hydrodynamics processor (SPH), a meshless Lagrangian technique appropriate to brittle materials and used in these simulations. Clegg et al. (2002) demonstrated the role of early shear failure and material comminution in the location and forward propagation of cracks in brittle materials subjected to hypervelocity impact and emphasize that the final damage state of their brittle target material depended not only on its compressive thermodynamic and shear response during penetration but also on tensile behavior, especially in areas away from the high pressure region ahead of the penetrating projectile.

McDonnell et al. (2001) performed a suite of laboratory experiments and numerical simulations using AUTODYN-2D version 4.1.09 to investigate the timing and growth mechanisms of LEO hypervelocity impact fractures in HST

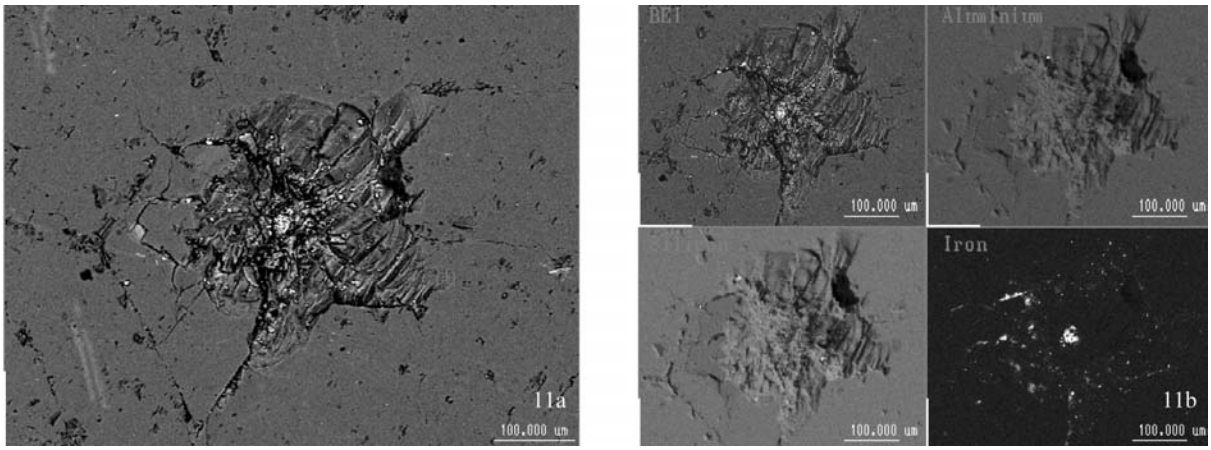

Fig. 11. a) BEI of crater on a polished surface of feldspathic gneiss, generated by impact of a small kamacite particle (38–58 µm diameter) moving at ~5 km s^{-1} in a light gas gun. The scale bar is 100 µm; b) EDS X-ray maps of an enlarged central area show concentration of projectile metal melt within the central pit and dispersion of brecciated target sulfide grains along radial fractures. The scale bar is 100 µm.

solar cell glass. For the solar cell impact simulations, the general approach described by Taylor et al. (1999) was employed, along with the Johnson-Holmquist failure model and specific parameters of 1.5×10^5 GPa tensile failure stress, 1×10^{20} GPa maximum shear stress, 1×10^4 Gf (MJ/m^2) crack softening, and erosion model strain set at 2. The modelled projectile was a 50 µm-diameter glass sphere impacting onto a target of glass with semi-infinite thickness at a velocity of 4 km s^{-1}. The study revealed that deep-penetrating fractures can be generated at a very early stage in the impact process, before rebound of the crater floor and ejection of the bulk of remnants of the impacting body (Fig. 12). Extensive shallow fracturing at a distance of several transient crater radii may occur over a slightly longer time scale. The progression of fracture development illustrated by the model revealed a mechanism that could account for the sequence of events necessary for emplacement of residue. The model fractures show good correspondence in position and orientation to locations in which we have observed residue in both space-exposed craters and laboratory light gas gun impacts, and the relative timing of projectile dispersion and fracture development seen within the model can account for the retention of debris. "Tagging" of different parts of the projectile during the simulation to determine which are retained, and in what shock state, was not performed but might have yielded important information.

The low hydrostatic pressure experienced within the substrate of small glass craters is very different from the kilobars of confining pressure that characterize the deep basement below large terrestrial craters. Thus, the role of tensile failure is likely to be a much smaller contribution to fracture development in the deep structure of very large craters (transient craters <5 km-diameter), and shear deformation will dominate except within the shallower margins of the crater. With this consideration, we suggest, nevertheless, that the creation of fractures in large (km-scale) craters is worthy of high priority in future modelling and that the location of residue-bearing fractures within terrestrial craters should be considered an important feature for correlation with models and in assessment of their applicability to real large craters.

DISCUSSION

Numerous authors, especially Melosh (1989, and many other seminal papers), have shown that numerical modelling can be remarkably successful in the simulation of major features in crater development and can account for many of the structures recognized during examination of larger terrestrial craters (e.g., Melosh and Ivanov 1999; Pierazzo and Melosh 1999; Kenkmann et al. 2000), such as the formation of peak rings (Collins et al. 2002) and even tektite strewn fields (Stöffler et al. 2002). In the majority of these models, the target behavior during impact is likened to that of an unusual fluid, with the bulk rock properties considered to yield to "acoustic fluidization." The larger brittle features such as ring and radial fault systems and their associated pseudotachylites (Thompson and Spray 1994) have usually been assumed to be relatively late stage, formed during modification of the transient cavity, uplift of the crater floor, and collapse to create complex crater morphology. However, the significance of pervasive small (m-scale) brittle structures in and around terrestrial impact craters has also become apparent from field studies (Spray 1998; Kenkmann et al. 2000). The simulation of these critical features within numerical models has been restricted due to constraints upon representation of their fine scale that are imposed by computing capacity (Melosh 2003, personal communication), but their importance in determining the capability of large rock masses to behave as fluid media by small-scale shearing and frictional slip during crater formation has certainly been recognized (Collins et al. 2004). The occurrence of breccia-

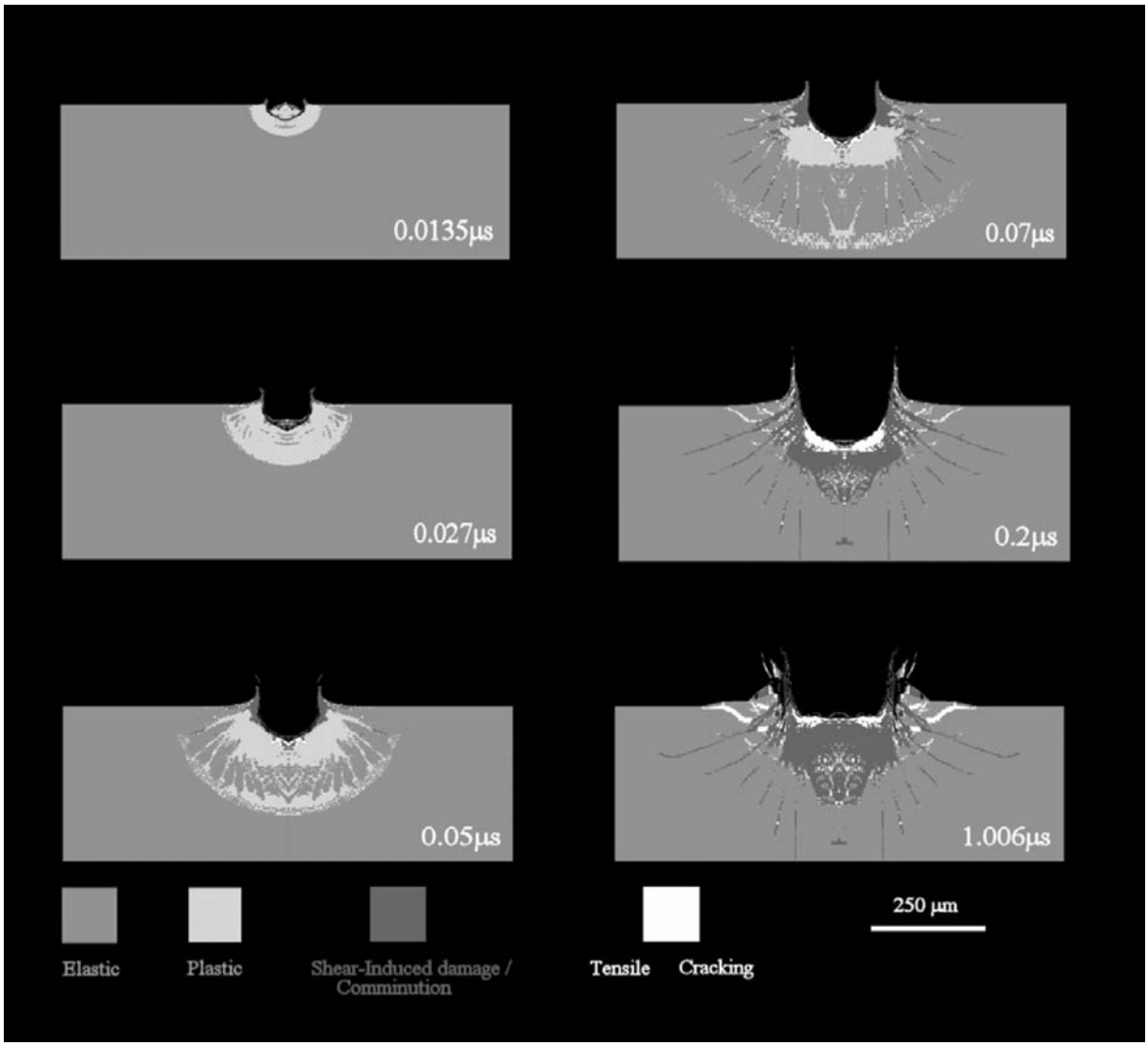

Fig. 12. Six timed frames from an AUTODYN-2D impact simulation of the first microsecond following contact of a 50 μm-diameter glass sphere moving at 4 km s^{-1} perpendicular to a glass surface (for more details of this simulation, see McDonnell et al. [2001]). The material state is described by color code. Note early strain localization and generation of well-defined zones of shear comminution and slightly later tensile cracking. The scale bar is 250 μm.

filled dykes and their potential as conduits for melt intrusion is also receiving more attention (Scott and Benn 2001). The role of brittle structures in subsequent crater modification is becoming clearer (Kenkmann et al. 2000; Kenkmann and von Dalwijk 2001). However, the difficulty of modelling the finest scale features, at which scale much brittle deformation has been noted in the field, has been a significant hurdle to numerical simulation. Detailed explanation of the origin of complex features such as radial fractures in the future will also require 3-dimensional modelling. Important questions that have not yet been fully addressed by models include the timing and location of major fracture development in relation to the availability and possible pathways of bolide residue material. Tracing tagged projectile material through the model into eventual emplacement or ejection would be particularly illuminating. The potential role of early-formed fractures in outward transport, thickening of the pre-impact stratigraphic sequence, and localization of structural weaknesses that permit subsequent inward crater collapse to form complex crater morphology may also prove to be very important.

SUMMARY

We believe that distinctive nickel-enriched metal residues can be used to track the presence of processed meteoritic metal. We have found that small grains and melt droplets can be emplaced within silicate impact melts, within vesicles in melts, and within fractures in both impact clasts and deeper into the basement. These observations imply that

the fractures must have been present at a stage when bolide remnants were still abundant. Evidence from both space-exposed and laboratory-simulated hypervelocity impacts of small projectiles suggests that small craters can develop extensive fracturing at an early stage when impactor residue is still available to be emplaced. Although we do not, and would not, suggest that the results of simulation from a mm-size crater should be scaled to km-size craters, our intriguing results suggest that emphasis on modelling the early fracturing of geological materials in larger, lithified, stratified target sequences may help to explain the distribution of residue emplacement in and around major craters. Such models may help to constrain the optimum sites for sampling around eroded craters. We also suggest that successful prediction of the location for early fracture development and residue emplacement might be an important criterion for the assessment of the validity of numerical models of crater formation.

Acknowledgments–We would like to thank D. Baker for the larger Barringer melt droplet specimens, Ron Hartmann for the samples from Monturaqui, E. Dransart for the samples from Lonar, J. Wells for preparation of the polished sections, Sara Russell for the loan of the polished specimen of Dar al Gani 400, Oxford Brookes University, the Natural History Museum (London) for the extensive use of electron microprobe facilities, G. Drolshagen (ESA/ESTEC, Noordwijk) for the use of Hubble Space Telescope solar cells, and M. Burchell (The University of Kent at Canterbury) for performing some of the light gas gun shots. This paper has benefited greatly from reviews by Gareth Collins and Christian Koeberl, to whom the authors are indebted.

Editorial Handling—Dr. E. Pierazzo and Dr. R. Herrick

REFERENCES

Bischoff A., Weber D., Clayton R. N., Faestermann T., Franchi I., Herpers U., Knie K., Korschinek G., Kubik P. W., Mayeda T. K., Merchel S., Michel R., Neumann S., Palme H., Pillinger C. T., Schultz L., Sexton A. S., Spettel B., Verchovsky A. B., Weber H. W., Weckwerth G., and Wolf D. 1998. Petrology, chemistry, and isotopic compositions of the lunar highland regolith breccia Dar al Gani 262. *Meteoritics & Planetary Science* 33:1243–1257.

Bland P. A. and Artemieva N. A. 2003. Efficient disruption of small asteroids by the Earth's atmosphere. *Nature* 424:288–291.

Brett R. 1967. Metallic spherules in impactite and tektite glasses. *American Mineralogist* 52:721–733.

Brink M. C., Waanders F. B., and Bischoff A. A. 1997. Vredefort: A model for the anatomy of an astrobleme. *Tectonophysics* 270:83–114.

Bunch T. E. and Cassidy W. A. 1972. Petrographic and electron microprobe study of the Monturaqui impactite. *Contributions to Mineralogy and Petrology* 36:95–112.

Clegg R. A. and Hayhurst C. J. 2000. Numerical modeling of the compressive and tensile response of brittle materials under high pressure dynamic loading. *American Institute of Physics Conference Proceedings* 505:321–324.

Clegg R. A., Hayhurst C. J., and Robertson I. 2002. Development and application of a Rankine plasticity model for improved prediction of tensile cracking in ceramic and concrete materials under impact. In *Behavior of materials at high strain rates: Numerical modelling,* edited by Benitez F. G. Saint Louis (France): DYMAT. pp. 67–76.

Chao E. C. T. and El Goresy A. 1977. Shock attenuation and the implantation of Fe-Cr-Ni veinlets in the compressed zones of the 1973 Ries Research deep drill core. *Geologica Bavarica* 75:289–304.

Collins G. S., Melosh H. J., Morgan J. V., and Warner M. R. 2002. Hydrocode simulations of Chicxulub Crater collapse and peak-ring formation. *Icarus* 157:24–33.

Collins G. S., Melosh H. J., and Ivanov B. A. 2004. Modeling damage and deformation in impact simulations. *Meteoritics & Planetary Science*. This issue.

Degenhardt J. J., Buchanan P., Reid A. M., and Miller R. M. 1994. Breccia veins and dykes associated with the Roter Kamm crater, Namibia. In *Large meteorite impacts and planetary evolution,* edited by Dressler B. O, Grieve R. A. F., and Sharpton V. L. Special Paper 293. Boulder: Geological Society of America. pp. 197–208.

El Goresy A. and Chao E. C. T. 1976. Evidence of the impacting body of the Ries crater—The discovery of Fe-Cr-Ni veinlets below the crater bottom. *Earth and Planetary Science Letters* 31:330–340.

Fredriksson K., Dube A., Milton D. J., and Balasundaram M. S. 1973. Lonar Lake, India: An impact crater in basalt. *Science* 180:862–864.

Fredriksson K., Brenner P., Dube A., Milton D. J., Mooring C., and Nelen J. A. 1979. Petrology, mineralogy, and distribution of Lonar (India) and lunar impact breccias and glasses. *Smithsonian Contributions to Earth Sciences* 22:862–864.

French B. M. 1998. *Traces of catastrophe: A handbook of shock metamorphic effects in terrestrial impact structures.* Contribution No. 954. Houston: Lunar and Planetary Institute. 120 p.

Graham G. A., Kearsley A. T., Grady M. M., Wright I. P., Griffiths A. D., and McDonnell J. A. M. 2000. The collection of micrometeoroid remnants from low Earth orbit. *Advances in Space Research* 25:303–307.

Grieve R. A. F. 1992. Projectile identification in impact melts. *Meteoritics* 27:324.

Grieve R. A. F. and Dence 1979. The terrestrial cratering record II. The crater production rate. *Icarus* 38:230–242.

Horn N. P. and El Goresy A. 1980. The Rochechouart crater in France: Stony and not iron meteorite? Proceedings, 11th Lunar and Planetary Science Conference. pp. 486–470.

Hörz F., Mittlefehld D. W., and See T. H. 1991. Dissemination and fractionation of projectile material in impact melts from the Wabar crater, Saudi Arabia. *Meteoritics* 26:346–347.

Housley R. M. 1979. A model for chemical and isotopic fractionation in the lunar regolith produced by impact vaporization. Proceedings, 10th Lunar and Planetary Science Conference. pp. 1673–1683.

Howard K. A., Offield T. W., and Wilshire H. G. 1972. Structure of Sierra Madera, Texas as a guide to central peaks of lunar craters. *Geological Society of America Bulletin* 83:2795–2808.

Hughes D. W. 2000. The terrestrial cratering rate over the last 125 million years. In *Impacts and the early Earth,* edited by Gilmour I. and Koeberl C. Berlin: Springer Verlag. pp. 327–341.

Hüttner R. and Schmidt-Kaler H. 1999. Erlauterungen zur Geologische Karte des Rieses 1:50,000. *Geologica Bavarica* 104:7–76.

Kelly W. R., Holdsworth E., and Moore C. B. 1974. The chemical composition of metallic spheroids and metallic particles within

impactite from Barringer meteorite crater, Arizona. *Geochimica et Cosmochimica Acta* 38:533–543.

Kenkmann T. and von Dalwigk I. 2000. Radial transpression ridges: A new structural feature of complex impact craters. *Meteoritics & Planetary Science* 35:1189–1202.

Kenkmann T., Ivanov B. A., and Stoffler D. 2000. Identification of ancient impact structures: Low-angle normal faults and related geological features of crater basements. In *Impacts and the early Earth,* edited by Gilmour I. and Koeberl C. Berlin: Springer Verlag. pp. 271–309.

Koeberl C. 1998. Identification of meteoritical components in impactites. In *Meteorites: Flux with time and impact effects,* edited by Grady M. M, Hutchison R., McCall G. J. H., and Rothery D. A. Special Publication 140. London: Geological Society of London. pp. 133–152.

Koeberl C. 2001. The sedimentary record of impact events. In *Accretion of extraterrestrial matter throughout Earth's history,* edited by Peucker-Ehrenbrink B. and Schmitz B. Amsterdam: Kluwer. pp. 333–378.

Koeberl C. and Reimold W. U. 2003. Geochemistry and petrology of impact breccias and target rocks from the 145 Ma Morokweng impact structure, South Africa. *Geochimica et Cosmochimica Acta* 67:1837–1862.

Koeberl C., Sharpton V. L., Schurayt S. B., Shirey S. B., Blum J. B., and Marin L.E. 1994. Evidence for a meteoritic component in impact melt rock from the Chicxulub structure. *Geochimica et Cosmochimica Acta* 58:1679–1684.

Koeberl C., Reimold W. U., and Shirey S. B. 1996. A Re-Os isotope and geochemical study of the Vredefort granophyre: Clues to the origin of the Vredefort structure, South Africa. *Geology* 24:913–916.

Koeberl C., Armstrong R. A., and Reimold W. U. 1997. Morokweng, South Africa: A large impact structure of Jurassic-Cretaceous boundary age. *Geology* 25:731–734.

Koeberl C., Hough R. M., Boamah D., French B. M., McDonald I. and Reimold W. U. 2001. Woodleigh impact structure, Australia: Shock petrography and geochemical studies (abstract). *Meteoritics & Planetary Science* 36:101.

Koeberl C., Peucker-Ehrenbrink B., Reimold W. U., Shukolyukov A., and Lugmair G. W. 2002. A comparison of the osmium and chromium isotopic methods for the detection of meteoritic components in impactites: Examples from the Morokweng and Vredefort impact structures, South Africa. In *Catastrophic events and mass extinctions: Impacts and beyond,* edited by Koeberl C. and MacLeod K. G. Special Paper 356. Boulder: Geological Society of America. pp. 607–617.

Kremenetsky A. A. and Yushko N. A. 1997. Deep anatomy, composition, and evolution of large meteorite impacts: Scientific drilling data on the Puchezh-Katunki astrobleme, Russia (abstract). In *Conference on large meteorite impacts and Planetary Evolution (Sudbury 1997).* Contribution No. 922. Houston: Lunar and Planetary Institute. p. 29.

Krinov E. L. 1966. The Sikhote-Alin iron meteorite shower. In *Giant meteorites,* edited by Beynon M. M. New York: Pergamon Press. 266–376.

Kyte F. T. 1998. A meteorite from the Cretaceous/Tertiary boundary. *Nature* 396:237–239.

Kyte F. T. 2002. Unmelted meteoritic debris collected from Eltanin ejecta in Polarstern cores from expedition ANT XII/4. *Deep Sea Research II* 49:1063–1071.

Kyte F. T. and Brownlee D. E. 1985. Unmelted meteoritic debris in the late Pliocene Ir anomaly: Evidence for the impact of a non-chondritic asteroid. *Geochimica et Cosmochimica Acta* 49:1095–1108.

Masaitis V. L 1994. Impactites from Popigai crater. In *Large meteorite impacts and planetary evolution,* edited by Dressler B. O., Grieve R. A. F., and Sharpton V. L. Special Paper 293. Boulder: Geological Society of America. pp. 153–162.

McDonald I. 2002. Clearwater East impact structure: A re-interpretation of the projectile type using new platinum-group element data from meteorites. *Meteoritics & Planetary Science* 37:459–464.

McDonald I., Andreoli M. A. G., Hart R. J., and Tredoux M. 2001. Platinum-group elements in the Morokweng impact structure, South Africa: Evidence for the impact of a large ordinary chondrite projectile at the Jurassic-Cretaceous boundary. *Geochimica et Cosmochimica Acta* 65:299–309.

McDonnell J. A. M., Catling D. J., Herbert M. K., and Clegg R. A. 2001. Quasistatic to hypervelocity impactor loading of glass: AUTODYN hydrocode and static testing configurations. *International Journal of Impact Engineering* 26:487–496.

Melosh H. J. 1989. *Impact cratering: A geologic process.* Oxford: Oxford University Press.

Melosh H. J. and Ivanov B. A. 1999. Impact crater collapse. *Annual Review of Earth and Planetary Sciences* 27:385–415.

Mittlefehldt D. W., See T. H., and Hörz F. 1992. Dissemination and fractionation of projectile materials in the impact melts from Wabar crater, Saudi Arabia. *Meteoritics* 27:361–370.

Miura Y., Fukuyama S., Kedves M. A., Yamori A., Okamato M., and Gusik A. 1999. Chemical separation of Fe-Ni particles after impact. *Advances in Space Research* 25:285–288.

Morgan J. V. and Warner M. R. 1999. Chicxulub: The third dimension of a multi-ring impact basin. *Geology* 27:407–410.

Morgan J. V., Warner M. R., Collins G. S., Melosh H. J., and Christeson G. L. 2000. Peak-ring formation in large impact craters: Geophysical constraints from Chicxulub. *Earth and Planetary Science Letters* 183:347–354.

Morgan J. W., Janssens M. J., Hertogen J., Gros J., and Takahashi H. 1979. Ries Impact crater, southern Germany: Search for meteoritic material. *Geochimica et Cosmochimica Acta* 43:803–815.

O'Keefe J. D., Stewart S. T., Lainhart M. E., and Ahrens T. J. 2001. Damage and rock-volatile mixture effects on impact crater formation. *International Journal of Impact Engineering* 26:543–553.

Osinski G. R., Spray J. G., and Lee P. 2001. Impact-induced hydrothermal activity within the Haughton impact structure, arctic Canada: Generation of a transient warm, wet oasis. *Meteoritics & Planetary Science* 36:731–745.

Palme H. 1982. Identification of projectiles of large terrestrial impact craters and some implications for the interpretation of Ir-rich Cretaceous/Tertiary boundary layers. In *Geological implications of impacts of large asteroids and comets on Earth,* edited by Silver L. T. and Schultz P. H. Special Paper 190. Boulder: Geological Society of America. pp. 223–233.

Pernicka E., Horn P., and Pohl J. 1987. Chemical record of the projectile in the graded fall-back sedimentary unit from the Ries crater, Gemany. *Earth and Planetary Science Letters* 86:113–121.

Pierazzo E. and Melosh H. J. 1999. Hydrocode modelling of Chicxulub as an oblique impact event. *Earth and Planetary Science Letters* 165:163–176.

Rinehart J. S. 1957. Distribution of meteoritic debris about the Arizona meteorite crater. *Smithsonian Contributions to Astrophysics* 2:145–160.

Sanchez J. and Cassidy W. A. 1966. A previously undescribed meteorite crater in Chile. *Journal of Geophysical Research* 71: 4891–4895.

Schmidt G., Palme H., and Kratz K. L. 1995. The fractionation of highly siderophile elements (HSE) in impact melts and the determination of the meteoritic components. *Meteoritics* 30:573–574.

Schnabel C., Pierazzo E., Xue S., Herzog G. F., Masarik J., Cresswell R. G., di Tada M. L., Liu K., and Fifield L. K. 1999. Shock melting of the Canyon Diablo impactor: Constraints from nickel-59 measurements and numerical modelling. *Science* 285:85–88.

Scott R. G. and Benn K. 2001. The role of radial impact melt dykes in impact crater collapse: New insights from the Sudbury impact structure, Canada (abstract). *Meteoritics & Planetary Science* 36: 186.

Scott R. G. and Spray J. G. 2000. The South Range Breccia Belt of the Sudbury impact structure: A possible terrace collapse feature. *Meteoritics & Planetary Science* 35:505–520.

Shoemaker E. M. and Kieffer S. W. 1974. *Guidebook to the geology of Meteor Crater, Arizona*. Publication 17. Tempe: Arizona State University, Center for Meteorite Studies. 66 p.

Spencer L. J. and Hey M. H. 1933. Meteoric iron and silica-glass from the meteorite craters of Henbury (central Australia) and Wabar (Arabia). *Mineralogical Magazine* 23:387–404.

Spray J.G. 1998. Localized shock- and friction-induced melting in response to hypervelocity impact. In *Meteorites: Flux with time and impact effects,* edited by Grady M. M., Hutchison R., McCall G. J. H., and Rothery D. A. Special Publication 140. London: Journal of the Geological Society of London. pp. 171–180.

Spray J. G. 2001. Impact and Friction-generated dykes of the Sudbury impact structure: Windows into excavation and modification phase processes (abstract). *Meteoritics & Planetary Science* 36: 195.

Stewart S. A. and Allen P. J. 2002. A 20 km-diameter multi-ringed impact structure in the North Sea. *Nature* 418:520–523.

Stöffler D., Bischoff L., Oskierski W., and Wiest B. 1988. Structural deformation, breccia formation, and shock metamorphism in the basement of complex terrestrial impact craters: Implications for the cratering process. In *Deep drilling in crystalline bedrock, vol. 1,* edited by Boden A. and Eriksson K. G. New York: Springer-Verlag. pp. 277–297.

Stöffler D., Artemieva N. A, and Pierazzo E. 2002. Modeling the Ries-Steinheim impact event and the formation of the moldavite strewn field. *Meteoritics & Planetary Science* 37: 1893–1907.

Sugita S., Kadono T., Ohno S., Hamano K., and Matsui T. 2003. Does laser ablation vapor simulate impact vapor? (abstract #1573). 34th Lunar and Planetary Science Conference. CD-ROM.

Taylor E. A., Hayhurst C. J., and Tsembelis K. 1999. Hydrocode modelling of space debris hypervelocity impact on soda-lime glass using the Johnson-Holmquist brittle material model. In *Proceedings of the Second European Conference on Space Debris.* Special Publication 393. Noordwijk: European Space Agency. pp. 449–453.

Taylor E. A., Scott H. J., Abraham M., and Kearsley A. T. 2001. Hypervelocity impact on silicon wafers with metallic and polymeric coatings. In *Proceedings of the Third European Conference on Space Debris.* Special Publication 473. Noordwijk: European Space Agency. pp. 583–590.

Thompson L. M. and Spray J. G. 1994. Pseudotachyltic rock distribution and genesis within the Sudbury impact structure. In *Large meteorite impacts and planetary evolution,* edited by Dressler B. O., Grieve R. A. F., and Sharpton V. L. Special Paper 293. Boulder: Geological Society of America. pp. 275–287.

Wittmann A., Kenkmann T., Schmitt R. T., and Stöffler D. 2003. Clastic polymict dykes in the megablock sequence of the ICDP-Chicxulub drill core YAX-1 (abstract #1386). 34th Lunar and Planetary Science Conference. CD-ROM.

Wood C. R. and Spray J. G. 1998. Origin and emplacement of offset dykes in the Sudbury impact structure: Constraints from Hess. *Meteoritics & Planetary Science* 33:337–347.

Yakovlev O. I. and Basilevsky A. T. 1994. Experimental studies of geochemical aspects of impact cratering. In L*arge meteorite impacts and planetary evolution,* edited by Dressler B. O., Grieve R. A. F., and Sharpton V. L. Special Paper 293. Boulder: Geological Society of America. pp. 73–80.

Zipfel J., Spettel B., Palme H., Franchi I., Sexton A. S., Pillinger C. T., and Bischoff A. 1998. Dar al Gani 400: Chemistry and petrology of the largest lunar meteorite (abstract). *Meteoritics & Planetary Science* 33:171.

Zolensky M. E. and Koeberl C. 1991 Why are blue zhamanshinites blue?: Liquid immiscibility in an impact melt. *Geochimica et Cosmochimica Acta* 55:1483–1486.